BOLETIN LATINOAMERICANO Y DEL CARIBE DE PLANTAS MEDICINALES Y AROMÁTICAS
© / ISSN 0717 7917 / www.blacpma.ms-editions.cl

Articulo Original / Original Article

Houttuynia cordata polysaccharide attenuates LPS-induced lung injury by inhibiting the HMGB3/JNK pathway through upregulation of miR-200b-3p

[El polisacárido de *Houttuynia cordata* atenúa la lesión pulmonar inducida por LPS inhibiendo la vía HMGB3/JNK mediante la regulación al alza de miR-200b-3p]

Wei Hong Liu[#], Li Yan Yin[#] & Bao Gang Wang

Department of Paediatrics, Shandong Provincial Third Hospital, Jinan City, Shandong Province, China
[#]**Equal contributions to this study**

Reviewed by:
Rafael Mex Alvarez
Universidad Autonoma de Campeche
Mexico

Miguel Avila
Universidad de Las Americas
Chile

Correspondence:
Bao Gang WANG
wangbaogangwbgg@outlook.com

Section Biotechnology

Received: 7 September 2024
Accepted: 16 March 2025
Accepted corrected: 7 May 2025
Published: 30 September 2025

Citation:
Liu WH, Yin LY, Wang BG. Houttuynia cordata polysaccharide attenuates LPS-induced lung injury by inhibiting the HMGB3/JNK pathway through upregulation of miR-200b-3p
Bol Latinoam Caribe Plant Med Aromat
24 (5): 790 - 814 (2025)
https://doi.org/10.37360/blacpma.25.24.5.55

Abstract: The aim was to investigate the therapeutic effects and molecular mechanisms of *Houttuynia cordata* polysaccharide (HCP) on LPS-induced lung injury. Effects were analyzed by HE, TUNEL, ELISA, MTT, and flow cytometry. Roles and mechanisms of HCP, miR-200b-3p, HMGB3, and JNK were studied by RT-qPCR, Western Blot, transfection, and dual luciferase reporter gene. HCP treatment effectively ameliorated LPS-induced lung injury in mice and TC-1 cells and was able to inhibit inflammatory factors as well as apoptosis with an effect close to that of dexamethasone-positive control. miR-200b-3p expression was down-regulated in LPS-induced lung injury and up-regulated by HCP treatment, and miR-200b-3p inhibitors reduced the therapeutic effects of HCP. miR-200b-3p targeted and negatively regulated HMGB3. HMGB3 was able to activate the JNK pathway to suppress the therapeutic effects of HCP on lung cell injury.HCP attenuates LPS-induced lung injury by upregulating miR-200b-3p to inhibit the HMGB3/JNK pathway.

Keywords: *Houttuynia cordata* polysaccharide; LPS-induced lung injury; Pneumonia; miR-200b-3p; HMGB3/JNK pathway.

Resumen: El objetivo fue investigar los efectos terapéuticos y los mecanismos moleculares del polisacárido de *Houttuynia cordata* (HCP) en la lesión pulmonar inducida por LPS. Los efectos se analizaron mediante HE, TUNEL, ELISA, MTT y citometría de flujo. Los roles y mecanismos de HCP, miR-200b-3p, HMGB3 y JNK se estudiaron mediante RT-qPCR, Western blot, transfección y ensayo de doble reportero luciferasa. El tratamiento con HCP mejoró eficazmente la lesión pulmonar inducida por LPS en ratones y células TC-1, e inhibió factores inflamatorios así como la apoptosis con un efecto cercano al del control positivo con dexametasona. La expresión de miR-200b-3p se reguló a la baja en la lesión pulmonar inducida por LPS y se reguló al alza con el tratamiento de HCP, mientras que los inhibidores de miR-200b-3p redujeron los efectos terapéuticos de HCP. miR-200b-3p se dirigió y reguló negativamente a HMGB3. HMGB3 fue capaz de activar la vía JNK para suprimir los efectos terapéuticos de HCP en la lesión celular pulmonar. HCP atenúa la lesión pulmonar inducida por LPS al regular al alza miR-200b-3p para inhibir la vía HMGB3/JNK.

Palabras clave: Polisacárido de *Houttuynia cordata*; Lesión pulmonar inducida por LPS; Neumonía; miR-200b-3p; vía HMGB3/JNK

INTRODUCTION

Pneumonia is a common infectious disease with high morbidity and mortality in children (Wang *et al*., 2021b). Pneumonia is usually treated with macrolide antibiotics, fluoroquinolones, and tetracyclines (Postma *et al*., 2015). Although drugs are now available for the treatment of pneumonia in children, however, antibiotic drugs have significant side effects and are prone to drug resistance. Therefore, finding effective treatments for pneumonia and reducing the incidence of lung injury and other complications has become a hot research topic.

Natural medicines with few side effects and easy accessibility highlight significant advantages in the treatment of pneumonia. *Houttuynia cordata*, an herbal medicine for the treatment of bacterial and viral pneumonia, contains a variety of compounds with antiviral, antifungal, detoxifying and antibacterial properties (Cheng *et al*., 2014; Chun *et al*., 2014; Lee *et al*., 2015; Cheng *et al*., 2019). The plant has been used to treat diseases such as pneumonia, lung abscess, dysentery, fever, colds and mumps, and is known to enhance the immune barrier of various organs (Liu *et al*., 2022; Zhou *et al*., 2022; Ju *et al*., 2023). *Houttuynia cordata* polysaccharide (HCP) is an active ingredient extracted from Houttuynia cordata. The monosaccharide composition is mainly xylose, fructose, arabinose and galactose. HCP has a broad-spectrum antiviral effect and has different degrees of inhibition on a variety of viruses (Chen *et al*., 2019). It has been demonstrated that HCP can attenuate LPS-induced inflammatory lung injury, which is related to its inhibitory effect on complement and macrophage overactivation (Xu *et al*., 2015). Moreover, HCP has beneficial effects on acute lung injury and endotoxic fever in rats associated with anticomplementary activity (Lu *et al*., 2018). In addition, HCP improves the severity of pneumonia and intestinal injury in influenza virus-infected mice (Zhu *et al*., 2018).

MicroRNA (miRNA), as a kind of non-coding RNA, plays a gene regulatory role by recognizing the 3'untranslated region (3'UTR) of target mRNA (Ullah *et al*., 2014) and is involved in cell proliferation, differentiation, and apoptosis (Wang *et al*., 2020). Dysregulation of miRNAs has been identified as a diagnostic biomarker of pneumonia (Huang *et al*., 2017). miRNAs are associated with apoptosis and inflammation in alveolar epithelial cells (Li & Liu, 2020). For instance, overexpressing miR-874-3p could alleviate LPS-induced apoptosis and inflammation in alveolar epithelial cells (Yang *et al*., 2021).

High mobility group box (HMGB) proteins are extracellular endogenous molecules released after tissue injury (Taniguchi *et al*., 2018). High expression of HMGB3 exacerbates LPS-induced inflammation and apoptosis in human alveolar epithelial cells (Li *et al*., 2023). Overexpressing HMGB3 promotes apoptosis, inhibits cell viability, and activated inflammation in LPS-injured lung cells (Sun *et al*., 2021). Many studies have shown that HMGB is associated with the JNK signaling pathway (Yu *et al*., 2017; Wang *et al*., 2021a; Alaaeldin *et al*., 2023). However, HMGB3 regulation of the JNK pathway has rarely been studied.

Overall, the aim of this study was to investigate the potential therapeutic effects and molecular mechanisms of HCP on LPS-induced lung injury in children's pneumonia.

MATERIALS AND METHODS

Laboratory animals

Sixty male SPF-graded BALB/c mice (3-4 weeks old, weighing 17-19 g) were purchased from Esebio (Shanghai, China). Food and water were freely available to all mice, and all mice were maintained at constant temperatures and humidity. Animal experiments were performed with the approval of the Ethics Committee of the Shandong Provincial Third Hospital.

Establishment and grouping of LPS pneumonia mouse model

HCP (98% purity, Ci Yuan Biotechnology Co., LTD. Shaanxi, China) was dissolved in 5% carboxymethylcellulose sodium (CMC) solution and administered by oral gavage. Dexamethasone (DEX) was purchased from Sigma. The mice were randomly divided into control, LPS, LPS + DEX, LPS + L-HCP, and LPS + H-HCP groups, with 10 mice in each group. Both control and LPS groups were gavaged with 5% CMC for 21 consecutive days. HCP was administrated by daily gavage for 21 days at 20 mg/kg and 100 mg/kg for the LPS + L-HCP and LPS + HCP groups. The LPS + DEX group was subjected to a gavage of DEX solution at 100 mg/kg. On day 22, the control group received 100 μL normal saline, and other groups received 100 μL of LPS (6 mg/kg) by endotracheal instillation. Twenty-four hours after the last dose, mice were executed by carbon dioxide asphyxiation, and blood samples were collected by cardiac puncture and centrifuged at 3000 × g for 10

min to extract serum, which was stored at -80°C. A sterile intravenous catheter was inserted into the trachea, and BALF was collected by rinsing 3 times with 1 mL normal saline and centrifuged at 1000 rpm for 5 min. The collected supernatant was then stored at -80°C for subsequent ELISA analysis. Lung tissues from mice were collected and a portion of the lung tissue was fixed in 4% paraformaldehyde for histopathological evaluation and subsequent experiments. The other portion of lung tissue was quickly frozen in liquid nitrogen and stored at -80°C.

HE staining

Mouse lung tissue was fixed in 4% paraformaldehyde for 24 h, embedded in paraffin, and made into 5 mm cross-sectional sections. Lung sections were deparaffinized with xylene and then treated with different concentrations of ethanol for 5 min. The samples underwent staining using hematoxylin for 5 min, followed by a 1-min treatment with 5% acetic acid, and then a 1-min staining with eosin. After a dehydration process using 70%, 80%, 90%, and 100% ethanol for 10 s and xylene for one minute, the samples were sealed using neutral gum and examined under a Nikon microscope (Tokyo, Japan, ECLIPSE 90 i).

Cell culture

The mouse alveolar epithelial cell line, TC-1, was purchased from the American Type Culture Collection (VA, USA) and cultured in DMEM (Thermo Fisher, USA) with 10% FBS (Thermo Fisher) and 100 μL/mL penicillin and streptomycin (Beyotime, China) and placed at 37°C and 5% CO2. Cells were treated with 100 ng/mL LPS (Sigma, USA) for 6 h to mimic lung injury in vitro. The cells were grouped as follows: blank group (normal TC-1 cells), LPS group (100 ng/mL LPS-treated cells for 6 h), LPS + L-HCP group (cells in the LPS group were treated with 10 μg/ml HCP for 48 h), LPS + H-HCP group (cells in the LPS group were treated with 100 μg/ml HCP for 48 h).

Cell transfection

The coding sequence of the HMGB3 gene was cloned into a pcDNA3.1 vector (Invitrogen, Thermo Fisher Scientific). miR-200b-3p mimics, miR-200b-3p inhibitors, and corresponding negative controls were obtained from RiboBio (Guangzhou, China). Cells were cultured to 80-90% confluence and then transfected using Lipofectamine 3000 (Invitrogen). miR-200b-3p or HMGB3 was determined by RT-qPCR analysis.

RT-qPCR

Total RNA was isolated from TC-1 cells and lung tissues using TRIzol reagent (Invitrogen). cDNA synthesis was performed for miRNA by miRNA reverse transcription kit (TaKaRa). mRNA cDNA was produced utilizing the PrimeScript RT kit (TaKaRa). The RT-qPCR evaluation utilized the SYBR PrimeScript RT-PCR kit (TaKaRa) alongside the ABI 7500 real-time fluorescence quantitative PCR system (Agilent Technologies, USA). Either GAPDH or U6 served as the internal control. The comparative sum was determined using the 2-ΔΔCt technique. Table No. 1 displays the sequences of the primers.

Table No. 1
Primer sequences

Primers	Forward primers 5′-3′	Reverse primers 5′-3′
miR-200b-3p	TAATACTGCCTGGTAATGATGA	GCAGGGTCCGAGGTATTC
HMGB3 (mice)	TGGCTAAAGGTGACCCCAAG	CCAATGGAGATGCCAGGGTT
HMGB3 (human)	TCCGCCCCAAGATCAAATCC	GCTTTGCCGCCTTAGTGATG
GAPDH (mice)	CATCAACGGGAAGCCCATC	CTCGTGGTTCACACCCATC
GAPDH (human)	CACCCACTCCTCCACCTTTG	CCACCACCCTGTTGCTGTAG
U6	CTCGCTTCGGCAGCACA	AACGCTTCACGAATTTGCGT

ELISA

Tumor necrosis factor-α (TNF-α), interleukin-6 (IL-6), and interleukin-1 β (IL-1β) levels were assessed in mouse serum, BALF, and cell culture supernatants using ELISA kits (Abcam).

MTT assay

TC-1 cells underwent inoculation in 96-well plates (5 × 103 cells per well) over 48 h, with each well receiving an addition of 20 μL MTT (Sigma-Aldrich) for 4 h at 37°C. For a duration of 10 min, 150 μL

Dimethyl sulfoxide was combined, followed by measuring its optical density at 490 nm using a microplate reader (Bio-Rad, CA, USA)

Flow cytometry

The evaluation of apoptosis was conducted with the Annexin V-FITC/PI kit (BD Biosciences, CA, USA). Cell concentration was regulated to reach 1 × 106 cells per milliliter. The experiments utilized around 200 μL of a cell suspension, which was then reconstituted in 300 μL of binding buffer. Subsequently, the cells underwent staining using FITC (5 μL) and PI (5 μL) for half an hour at 25°C in darkness. The rate of apoptosis was measured using the flow cytometry system (BD company, Cowley, UK).

Dual luciferase reporter gene assay

The Targetscan database (**http://www.targetscan.org**) facilitated the prediction of possible binding sequences for miR-200b-3p with HMGB3 3'UTR. Subsequently, mutations were integrated into possible binding sequences utilizing a specialized mutagenesis kit (Stratagene, CA, USA). Both thewild-type (Wt) and mutant (Mut) binding sequences of HMGB3 were inserted into the pmirGLO vector (Promega, WI, USA). Using Lipofectamine 3000 reagent (Life Technologies), TC-1 cells underwent cotransfection with either a luciferase reporter gene vector, miR-200b-3p mimic, miR-200b-3p inhibitor, or their respective negative control (GenePharma, Shanghai, China). Post 48 h, the activity of luciferase was examined through a dual luciferase reporter gene assay system (Promega).

RIP

The EZ-Magna RIP kit (Millipore) was utilized to conduct RIP assays. TC-1 cells underwent transfection using mimic-NC or miR-200b-3p mimic for a duration of 48 h, followed by lysis in a full RIP lysis buffer. Then, 100 μL of cell extracts underwent incubation with magnetic beads that included beads linked to either human anti-Ago2 antibody (Abcam) or mouse IgG (Abcam). The immunoprecipitated RNA underwent purification and was utilized in RT-qPCR for detecting HMGB3 expression.

Western Blot

Total protein was collected using radioimmunoprecipitation buffer (Beyotime). Proteins (30 μg) were separated by SDS-PAGE and then transferred to a PVDF membrane. The membrane was blocked and incubated with the following primary antibodies: anti-HMGB3 (#ab18256, Abcam), anti-JNK (#ab76125, Abcam), anti-p-JNK (#4668, Cell Signaling Technology), anti-p65 (#ab16502, Abcam), anti-p-p65 (#3033, Cell Signaling Techmology), anti-Cleaved caspase 3 (#ab2302, Abcam) and anti-β-actin (#ab8227, Abcam). After incubation with secondary goat anti-rabbit IgG H&L (#ab205718, Abcam) for 1 h, the membrane was detected by ECL Kit (Thermo Fisher) and quantified using Quantity One 4.6.2.

Statistical analysis

The data were presented as mean ± standard deviation from a minimum of three separate experiments. The analysis was conducted using GraphPad Prism 8.0 software. The statistical evaluations utilized the Student's t-test for comparing two groups, a one-way variance analysis for multiple comparisons, followed by Tukey's post hoc test. A *p*-value less than 0.05 was deemed to hold statistical significance.

RESULTS

HCP attenuates LPS-induced lung tissue injury in mice

We established an *in vivo* pneumonia model by administering LPS intratracheally and evaluated the therapeutic effect of HCP in LPS-induced lung injury. LPS stimulation significantly increased inflammatory cell infiltration and induced pulmonary edema. HCP treatment significantly alleviated the above pathological changes induced by LPS, and the effect of HCP treatment was more pronounced at a higher dose, close to that of the positive control DEX (Figures No. 1, No. 2, No. 3). ELISA demonstrated that LPS increased TNF-α, IL-6, and IL-1β in mouse serum and BALF, whereas HCP treatment decreased these inflammatory factors (Figures No. 4A and 4B). Western Blot analyzed that HCP treatment ameliorated the increase of apoptotic proteins cleaved caspase-3 caused by LPS (Figure No. 5). The above data prove that HCP has a therapeutic effect in the in vivo pneumonia model, which can alleviate the inflammatory pathology of lung tissue, reduce the expression of inflammatory factors and cell apoptosis, and at the same dose, HCP shows a therapeutic effect very close to that of DEX.

HCP attenuates LPS-induced lung tissue injury in mice

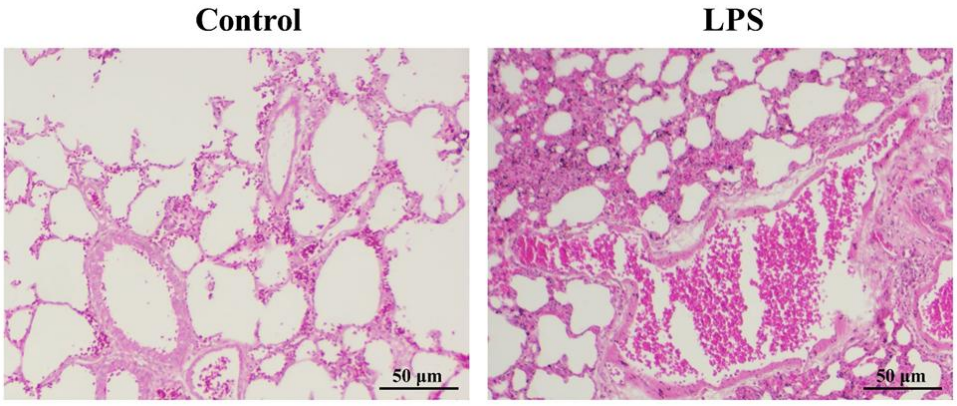

Figure No. 1
HE staining to observe the pathological damage of lung tissues

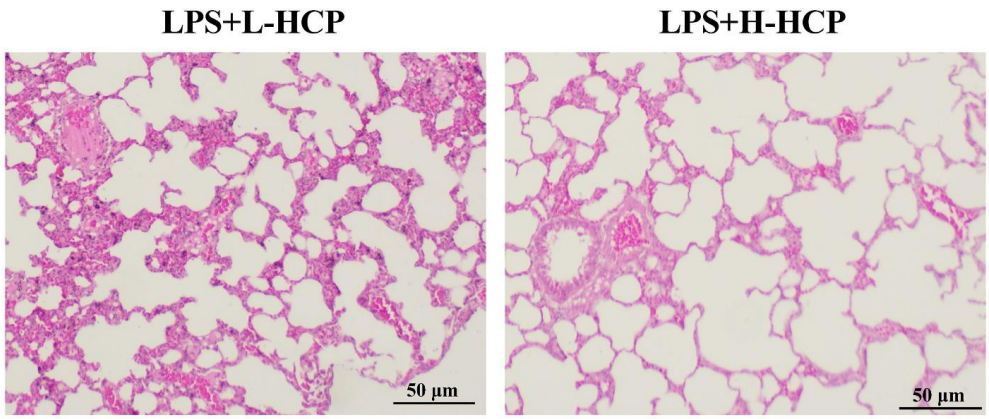

Figure No. 2
HE staining to observe the pathological damage of lung tissues

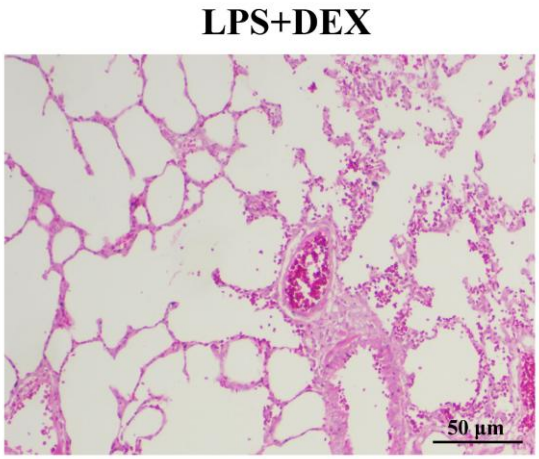

Figure No. 3
HE staining to observe the pathological damage of lung tissues

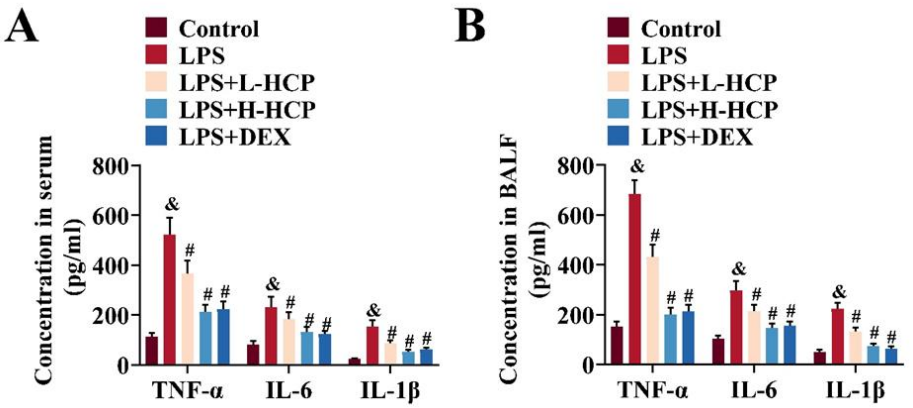

Figure No. 4
ELISA to detect the expression of inflammatory factors TNF-α, IL-6, and IL-1β in serum(A) and BALF(B) of mice. Data are expressed as mean ± SD (n=3). & vs. Control, *p*<0.05; # vs. LPS, *p*<0.05

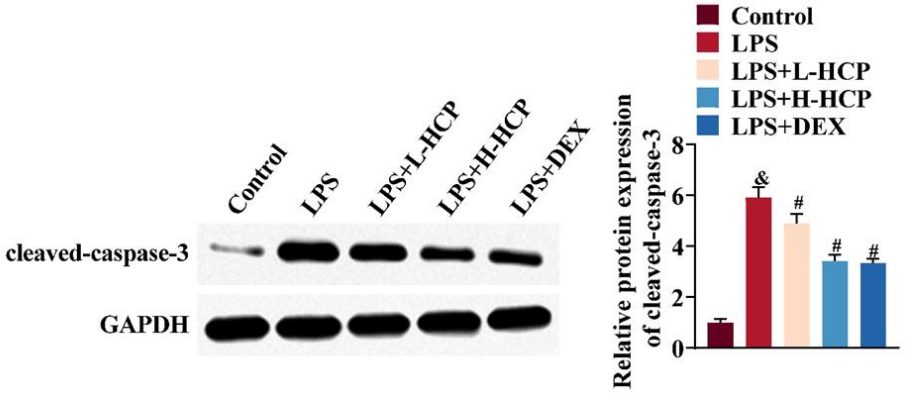

Figure No. 5
Western Blot to detect the expression of apoptotic protein cleaved caspase-3 in the lung tissues of mice. Data are expressed as mean ± SD (n=3). & vs. Control, *p*<0.05; # vs. LPS, *p*<0.05

HCP attenuates LPS-induced lung cell injury in vitro

An *in vitro* model for lung cell damage was created using LPS-activated TC-1 cells to explore HCP's role on lung cells. The ELISA findings indicated a notable rise in inflammatory agents TNF-α, IL-6, and IL-1β in TC-1 cell supernatant due to LPS, with HCP treatment markedly reducing these factors (Figure No. 6). MTT experiments determined that LPS stimulation decreased the cell viability of TC-1, and cellular HCP treatment revealed that the cell viability of TC-1 was restored in a dose-dependent manner (Figure No. 7). Flow cytometry results showed that HCP treatment was able to reverse the promotion of apoptosis by LPS (Figures No. 8, No. 9. No. 10). Western Blot results detected that LPS stimulation elevated cleaved caspase-3 in TC-1 cells, whereas HCP was able to down-regulate cleaved caspase-3 expression, and the down-regulation effect was more pronounced at high concentrations of HCP (Figure No. 11). In summary, HCP can improve LPS-induced lung cell injury, significantly reduce inflammatory indicators and apoptosis, and high-dose HCP shows the same therapeutic effect as DEX.

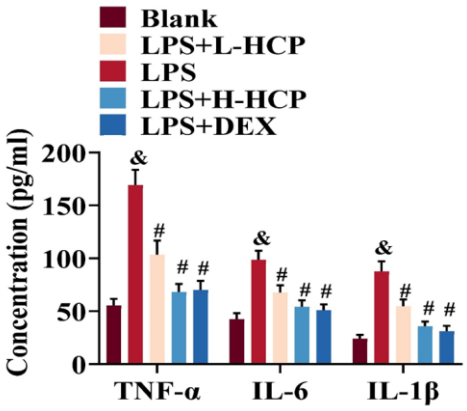

Figure No. 6
ELISA to detect inflammatory factors TNF-α, IL-6, and IL-1β in cells. Data are expressed as mean ± SD (n=3). & vs. Blank, $p<0.05$; # vs. LPS, $p<0.05$

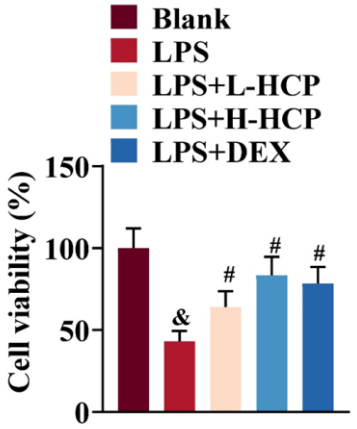

Figure No. 7
MTT to detect the cell viability.
Data are expressed as mean ± SD (n=3). & vs. Blank, $p<0.05$; # vs. LPS, $p<0.05$

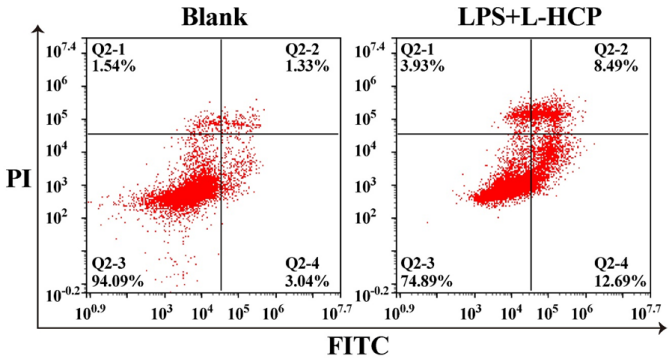

Figure No. 8
Flow cytometry to detect cell apoptosis.
Data are expressed as mean ± SD (n=3). & vs. Blank, $p<0.05$; # vs. LPS, $p<0.05$

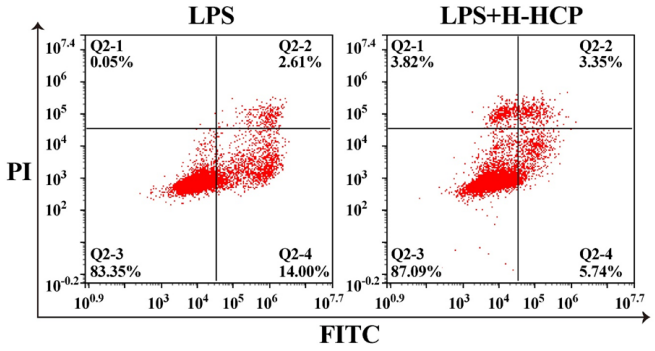

Figure No. 9
Flow cytometry to detect cell apoptosis.
Data are expressed as mean ± SD (n=3). & vs. Blank, *p*<0.05; # vs. LPS, *p*<0.05

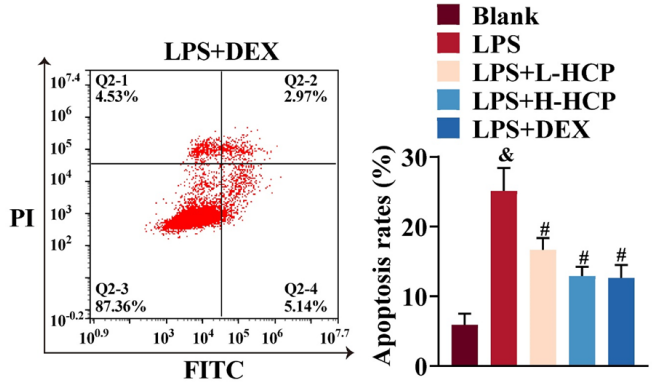

Figure No. 10
Flow cytometry to detect cell apoptosis.
Data are expressed as mean ± SD (n=3). & vs. Blank, *p*<0.05; # vs. LPS, *p*<0.05

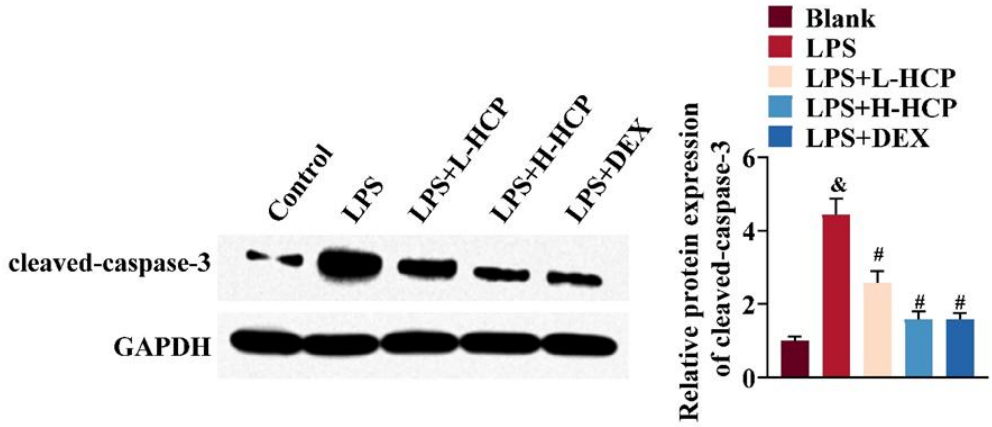

Figure No. 11
Western Blot to detect cleaved caspase-3 expression
Data are expressed as mean ± SD (n=3). & vs. Blank, *p*<0.05; # vs. LPS, *p*<0.05

miR-200b-3p knockdown downregulates the therapeutic effect of HCP on inflammatory injury in lung cells

miR-200b-3p was detected in mouse lung tissues and TC-1 cells using RT-qPCR. According to the results, miR-200b-3p showed low expression levels in LPS-induced injury in mouse lung tissues and TC-1 cells. After HCP treatment, its expression was restored (Figures No. 12A and No. 12B). TC-1 cells (LPS-treated and 100 μg/mL HCP-treated) were transfected with miR-200b-3p inhibitor, and the transfection efficiency was confirmed by RT-qPCR (Figure No. 13). As measured, the down-regulation of TNF-α, IL-6, and IL-1β by HCP was reversed by knockdown of miR-200b-3p (Figure No. 14). The therapeutic effect of HCP on cell viability was reversed by knockdown of miR-200b-3p (Figure No. 15). Flow cytometry results also showed that the restorative effect of HCP on LPS-induced apoptosis was reversed by knockdown of miR-200b-3p (Figures No. 16, No. 17 and No. 18). The down-regulation of cleaved caspase-3 by HCP was prevented by knockdown of miR-200b-3p (Figure No. 19). These data suggest that the therapeutic effect of HCP on LPS-induced lung cell inflammation and apoptosis may be related to the down-regulation of miR-200b-3p.

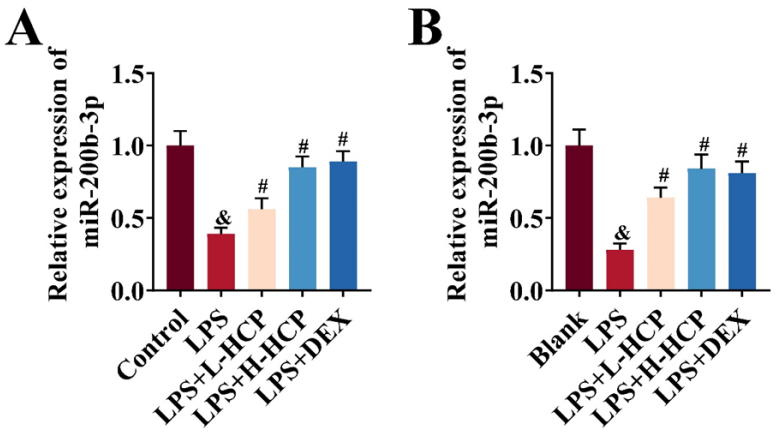

Figure No. 12
RT-qPCR to detect miR-200b-3p in mouse lung tissues and TC-1 cells
Data are expressed as mean ± SD (n=3). & vs. Control or Blank, $p<0.05$; # vs. LPS, $p<0.05$

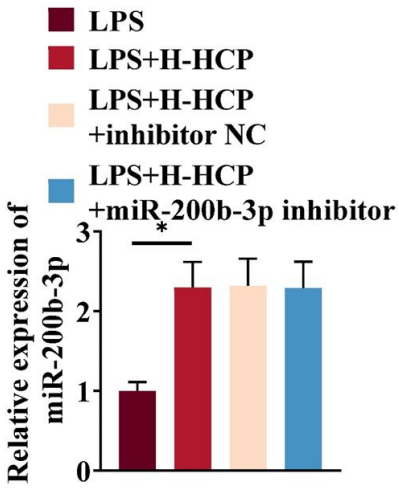

Figure No. 13
RT-qPCR to detect miR-200b-3p in cells after transfection with miR-200b-3p inhibitor
Data are expressed as mean ± SD (n=3). & vs. Control or Blank, $p<0.05$; # vs. LPS, $p<0.05$

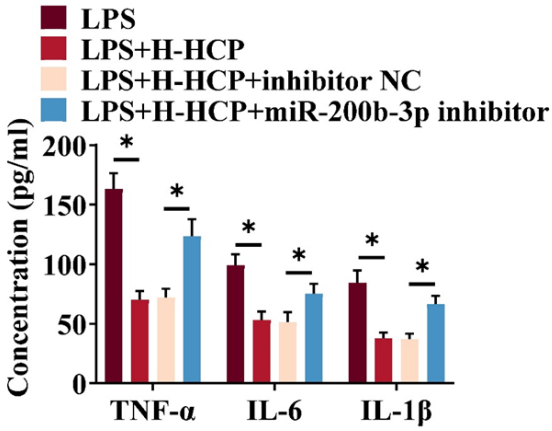

Figure No. 14
ELISA to detect TNF-α, IL-6, IL-1β levels
Data are expressed as mean ± SD (n=3). & vs. Control or Blank, *p*<0.05; # vs. LPS, *p*<0.05

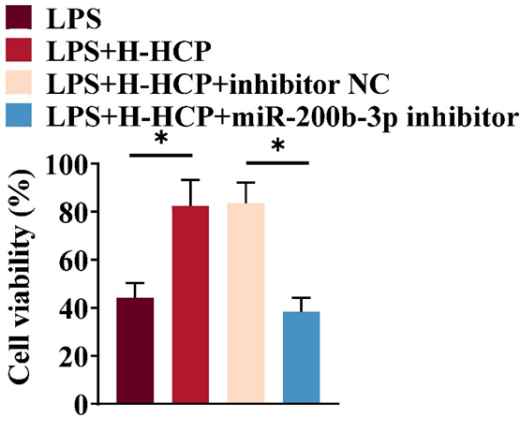

Figure No. 15
MTT to detect cell viability
Data are expressed as mean ± SD (n=3). & vs. Control or Blank, *p*<0.05; # vs. LPS, p<0.05

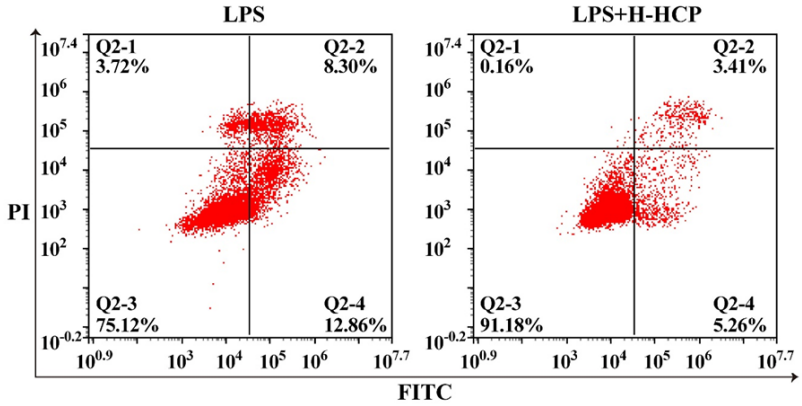

Figure No. 16
Flow cytometry to detect apoptosis
Data are expressed as mean ± SD (n=3). & vs. Control or Blank, *p*<0.05; # vs. LPS, *p*<0.05

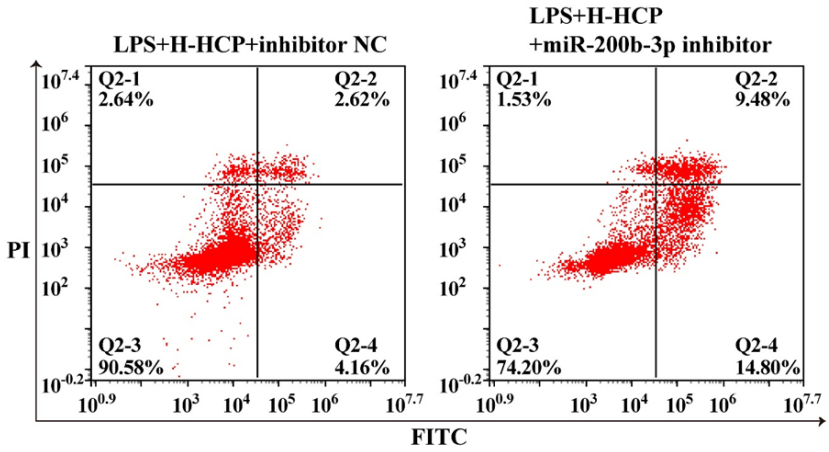

Figure No. 17
Flow cytometry to detect apoptosis
Data are expressed as mean ± SD (n=3). & vs. Control or Blank, *p*<0.05; # vs. LPS, *p*<0.05

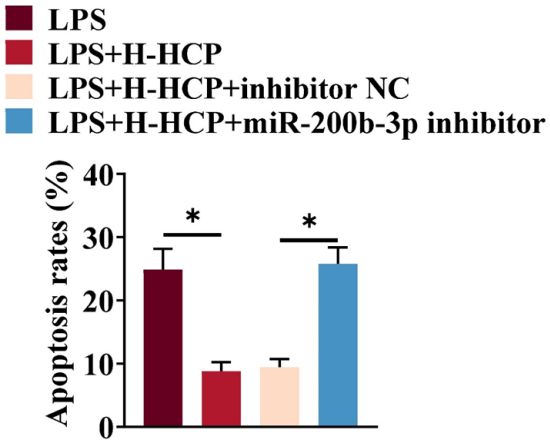

Figure No. 18
Flow cytometry to detect apoptosis
Data are expressed as mean ± SD (n=3). & vs. Control or Blank, *p*<0.05; # vs. LPS, *p*<0.05

Figure No. 19
Western Blot to detect cleaved caspase-3 in cells
Data are expressed as mean ± SD (n=3). & vs. Control or Blank, *p*<0.05; # vs. LPS, *p*<0.05

HMGB3 is a direct functional target of miR-200b-3p

The downstream mRNA of miR-200b-3p was investigated using the Targetscan database. HMGB3 was selected as the predicted binding target and its binding site with miR-200b-3p was predicted by starbase database (Figure No. 20). Then, HMGB3 was found to be significantly highly expressed in LPS-induced mouse lung tissues (Figures No. 21 and No. 22) and TC-1 cells (Figures No. 23 and No. 24) using RT-qPCR and Western Blot, and treatment with HCP was able to reduce HMGB3 expression. The existence of targeting between miR-150-5p and TRIM8 was further confirmed using a luciferase reporter gene assay. Co-transfection of miR-200b-3p mimics with WT-HMGB3 decreased the luciferase activity of cells (Figure No. 25A). the RIP assay showed that miR-200b-3p and TRIM8 were significantly enriched when using Ago2 antibody (Figure No. 25B). In addition, RT-qPCR and Western Blot determined that miR-200b-3p inhibitor upregulated HMGB3 expression, while miR-200b-3p mimic was able to inhibit HMGB3 expression (Figures No. 26 and No. 27). These results suggest that miR-200b-3p can target HMGB3, and the two are negatively regulated.

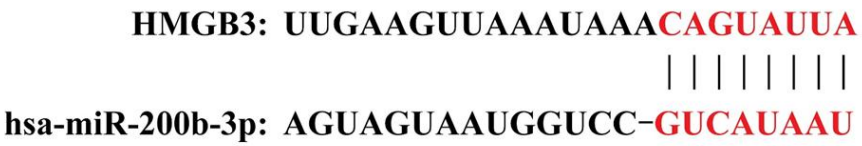

Figure No. 20
Targetscan predicts the binding site of HMGB3 to miR-200b-3p

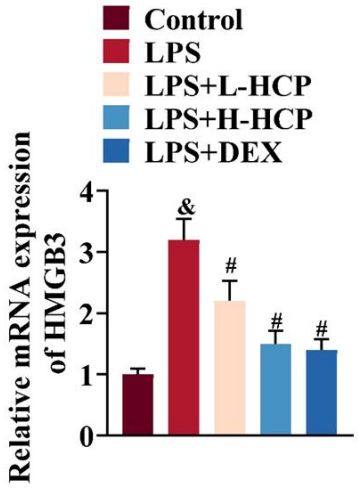

Figure No. 21
RT-qPCR and Western Blot to detect HMGB3 in mouse lung tissues
Data are expressed as mean ± SD (n=3). & vs. Control or Blank, $p<0.05$; # vs. LPS, $p<0.05$

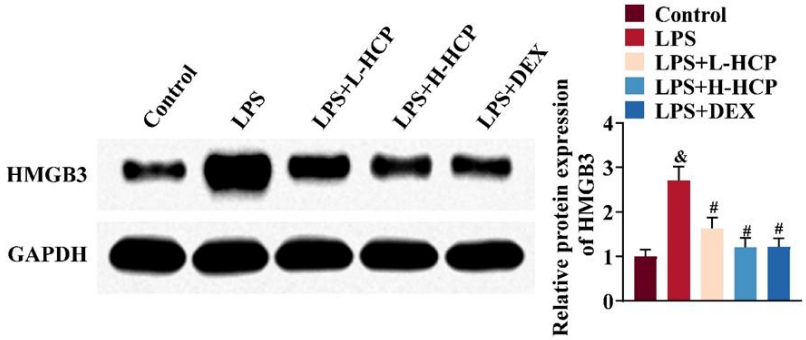

Figure No. 22
RT-qPCR and Western Blot to detect HMGB3 in mouse lung tissues
Data are expressed as mean ± SD (n=3). & vs. Control or Blank, $p<0.05$; # vs. LPS, $p<0.05$

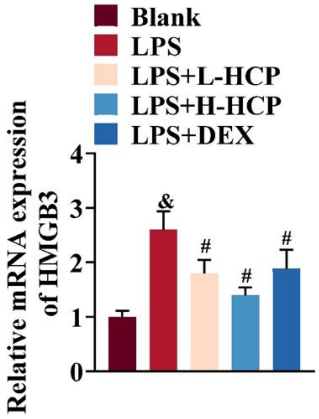

Figure No. 23
RT-qPCR and Western Blot to detect HMGB3 in TC-1 cells
Data are expressed as mean ± SD (n=3). & vs. Control or Blank, $p<0.05$; # vs. LPS, $p<0.05$

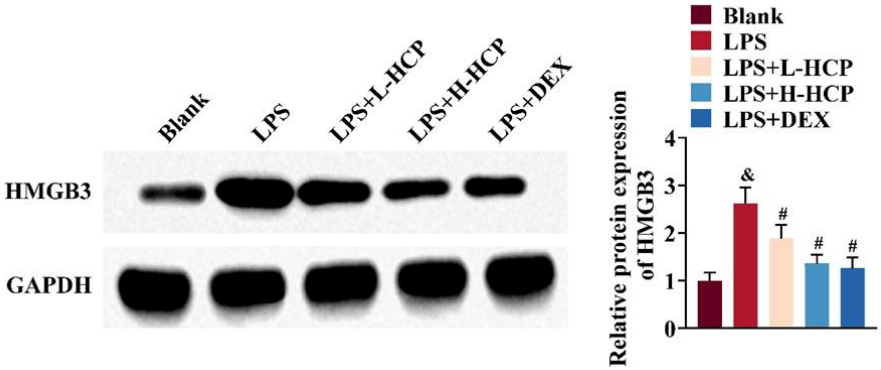

Figure No. 24
RT-qPCR and Western Blot to detect HMGB3 in TC-1 cells
Data are expressed as mean ± SD (n=3). & vs. Control or Blank, $p<0.05$; # vs. LPS, $p<0.05$

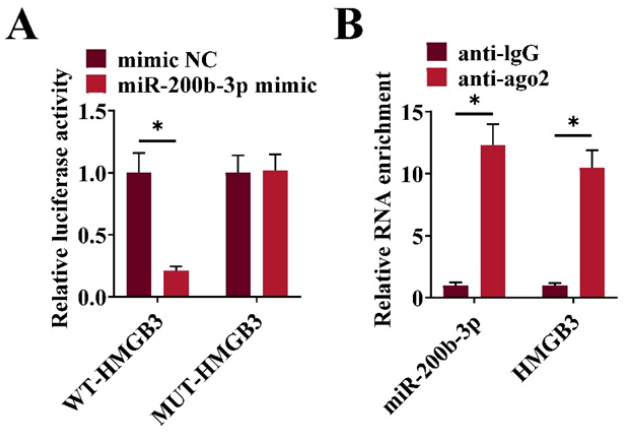

Figure No. 25

Dual luciferase reporter assay(A) and RIP(B) assay to verify the targeting relationship between miR-200b-3p and HMGB3. Data are expressed as mean ± SD (n=3). & vs. Control or Blank, $p<0.05$; # vs. LPS, $p<0.05$

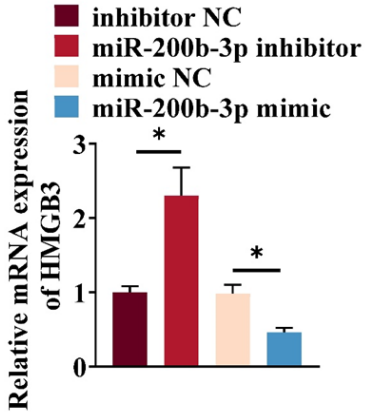

Figure No. 26

RT-qPCR and Western Blot to detect the effects of miR-200b-3p mimics and miR-200b-3p inhibitors on HMGB3 expression. Data are expressed as mean ± SD (n=3). & vs. Control or Blank, $p<0.05$; # vs. LPS, $p<0.05$

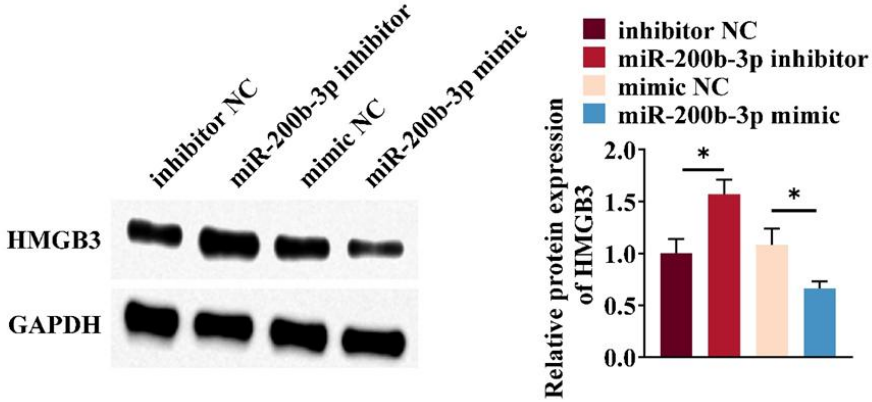

Figure No. 27

RT-qPCR and Western Blot to detect the effects of miR-200b-3p mimics and miR-200b-3p inhibitors on HMGB3 expression. Data are expressed as mean ± SD (n=3). & vs. Control or Blank, $p<0.05$; # vs. LPS, $p<0.05$

Overexpression of HMGB3 suppresses the therapeutic effect of miR-200b-3p upregulation on LPS-induced lung cell injury

TC-1 cells were transfected with miR-200b-3p mimic alone or miR-200b-3p mimic co-transfected with HMGB3 overexpression vector pcDNA3.1-HMGB3. RT-qPCR and Western Blot assays showed that HMGB3 in TC-1 cells was significantly increased after transfection with pcDNA3.1-HMGB3 (Figures No. 28 and No. 29). miR-200b-3p overexpression inhibited TNF-α, IL-1β, and IL-6, whereas upregulating HMGB3 upregulated their levels (Figure No. 30). The impact of miR-200b-3p overexpression on cell viability (Figure No. 31) and apoptosis (Figure No. 32, No. 33, No. 34 and No. 35) was reversed by HMGB3 overexpression. In summary, overexpression of HMGB3 can reverse the therapeutic effect of miR-200b-3p up-regulation on LPS-induced lung cell inflammation and apoptosis.

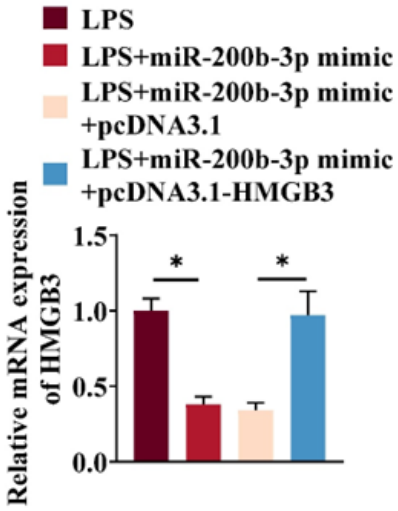

Figure No. 28
RT-qPCR and Western Blot to detect HMGB3 in TC-1 cells after transfection with pcDNA3.1-HMGB3
Data are expressed as mean ± SD (n=3). *p<0.05

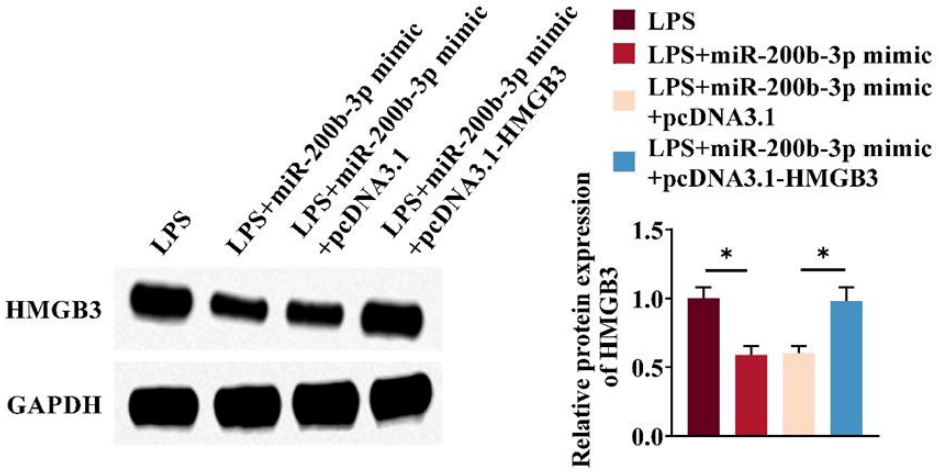

Figure No. 29
RT-qPCR and Western Blot to detect HMGB3 in TC-1 cells after transfection with pcDNA3.1-HMGB3
Data are expressed as mean ± SD (n=3). *p<0.05

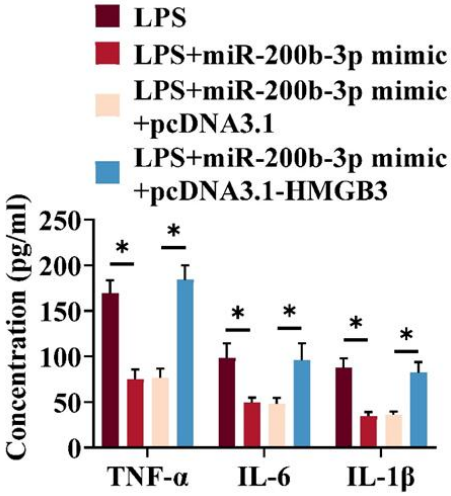

Figure No. 30
ELISA to detect TNF-α, IL-1β, and IL-6
Data are expressed as mean ± SD (n=3). *p<0.05

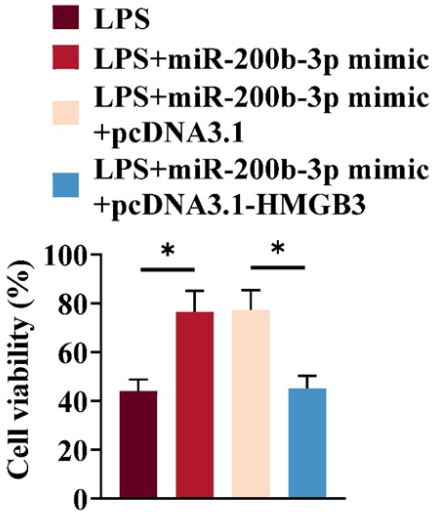

Figure No. 31
MTT to detect cell viability
Data are expressed as mean ± SD (n=3). *p<0.05

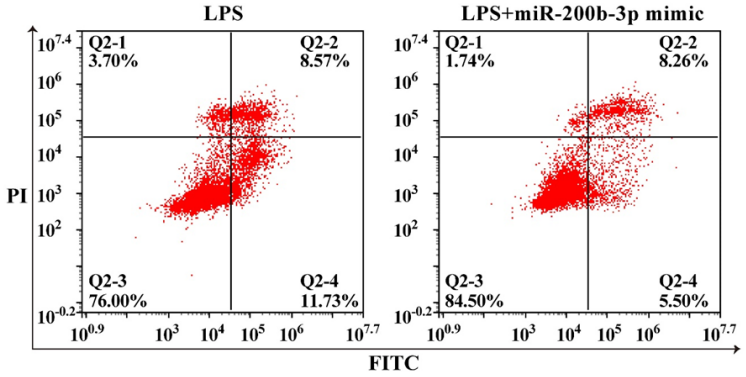

Figure No. 32
Flow cytometry to detect apoptosis
Data are expressed as mean ± SD (n=3). *p<0.05

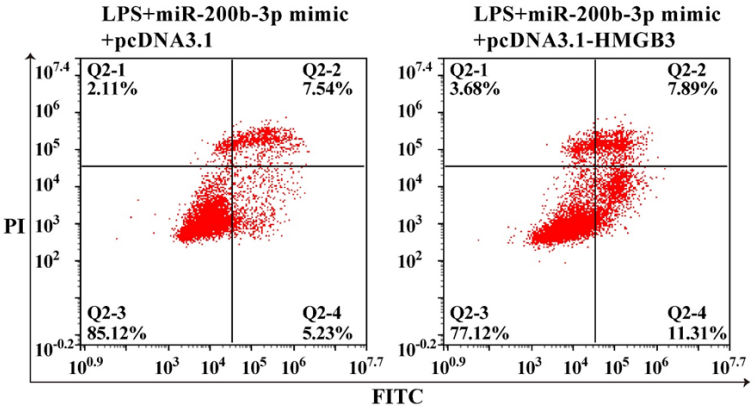

Figure No. 33
Flow cytometry to detect apoptosis
Data are expressed as mean ± SD (n=3). *p<0.05

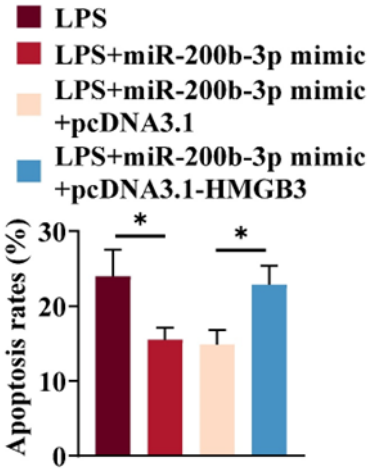

Figure No. 34
Flow cytometry to detect apoptosis
Data are expressed as mean ± SD (n=3). *p<0.05

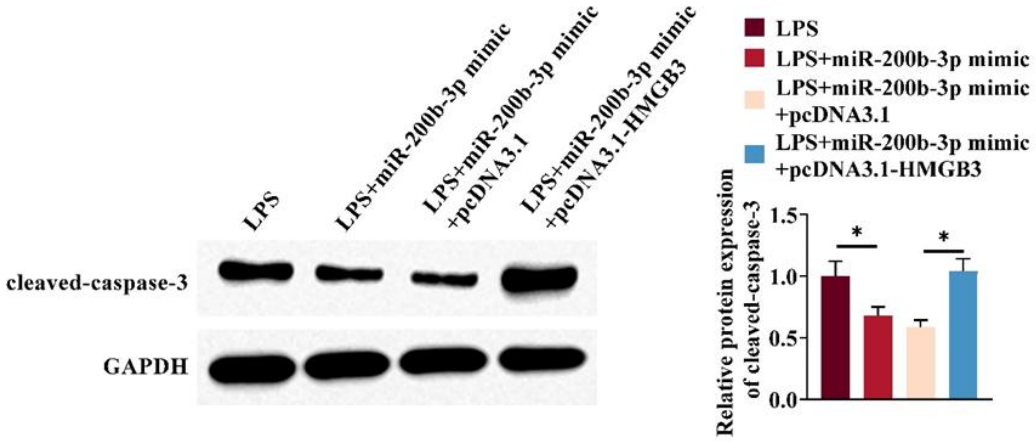

Figure No. 35
Western Blot to detect cleaved caspase-3 in TC-1 cells expression
Data are expressed as mean ± SD (n=3). *p<0.05

HMGB3 overexpression attenuates the therapeutic effect of HCP on lung cell injury by promoting JNK pathway activation

To further investigate whether the downstream JNK signaling pathway regulated by HMGB3 has an impact on the therapeutic effect of HCP on lung cell injury, LPS and 100 μg/mL HCP were applied to TC-1 cells and transfected with pcDNA3.1-HMGB3 to overexpress HMGB3. RT-qPCR and Western Blot assays showed that HMGB3 was significantly up-regulated in TC-1 cells after transfection with pcDNA3.1-HMGB3 (Figures No. 36 and No. 37). Meanwhile, Western Blot results also showed significant up-regulation of p-JNK and p-p65, indicating that JNK signaling was activated (Figure No. 38), but these effects were suppressed after HCP treatment. ELISA results showed that HCP was able to reduce TNF-α, IL-1β, and IL-6, whereas after overexpression of HMGB3 upregulated these three inflammatory factors (Figure No. 39). MTT experiments showed that the impact of HCP on TC-1 cell viability (Figure No. 40) and apoptosis (Figures No. 41, No. 42, No. 43 and No. 44) was reversed by overexpression of HMGB3. In summary, overexpression of HMGB3 attenuates the therapeutic effect of HCP on inflammation and apoptosis of lung cells by promoting the activation of JNK signaling pathway.

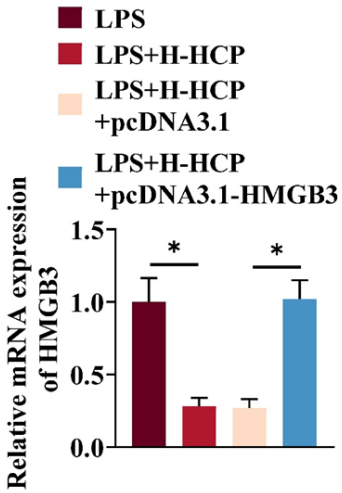

Figure No. 36
RT-qPCR and Western Blot to detect HMGB3 in the cells
Data are expressed as mean ± SD (n=3). *p<0.05

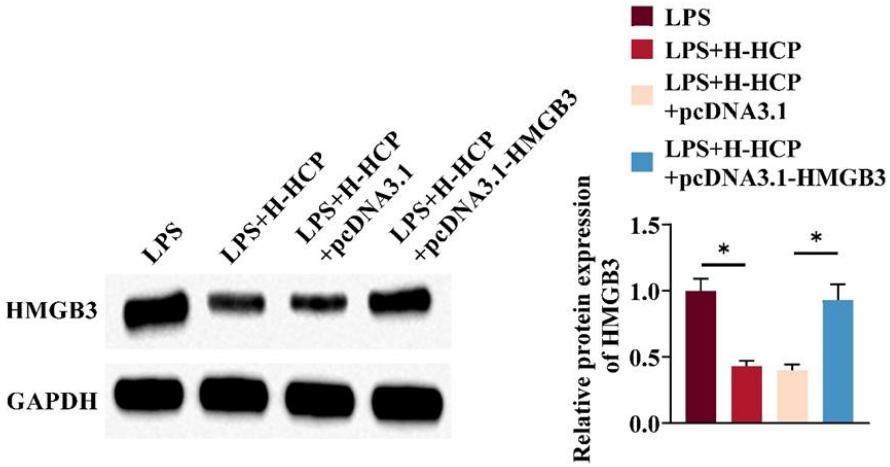

Figure No. 37
RT-qPCR and Western Blot to detect HMGB3 in the cells
Data are expressed as mean ± SD (n=3). *p<0.05

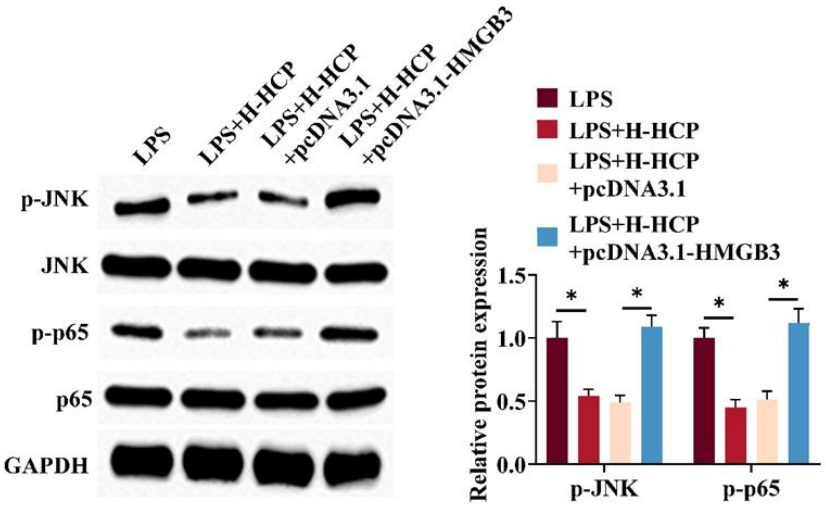

Figure No. 38
Western Blot to detect p-JNK and p-p65 in TC-1 cells
Data are expressed as mean ± SD (n=3). *p<0.05

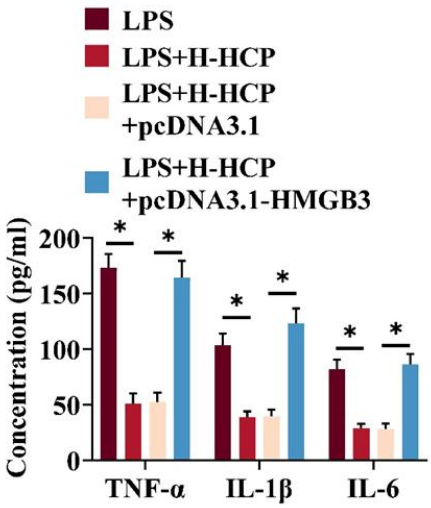

Figure No. 39
ELISA to detect TNF-α, IL- 1β and IL-6
Data are expressed as mean ± SD (n=3). *p<0.05

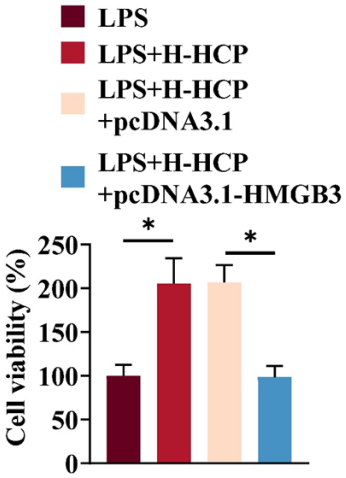

Figure No. 40
MTT detection of cell viability in TC-1
Data are expressed as mean ± SD (n=3). *p<0.05

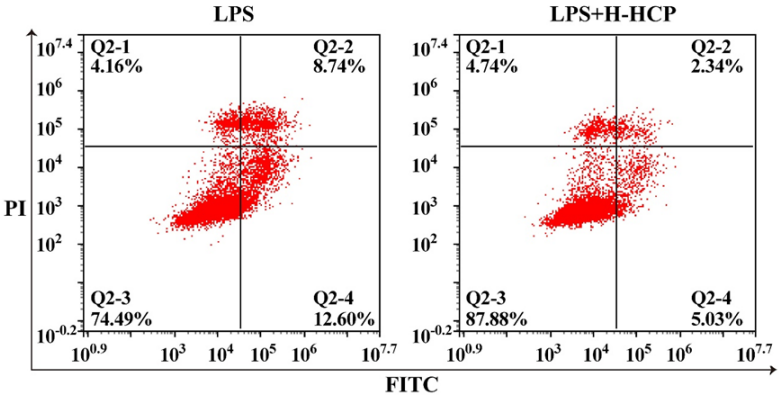

Figure No. 41
Flow cytometry detection of apoptosis in TC-1
Data are expressed as mean ± SD (n=3). *p<0.05

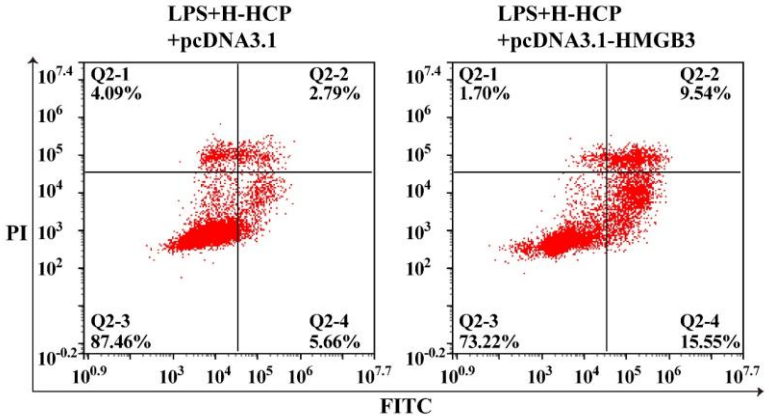

Figure No. 42
Flow cytometry detection of apoptosis in TC-1
Data are expressed as mean ± SD (n=3). *p<0.05

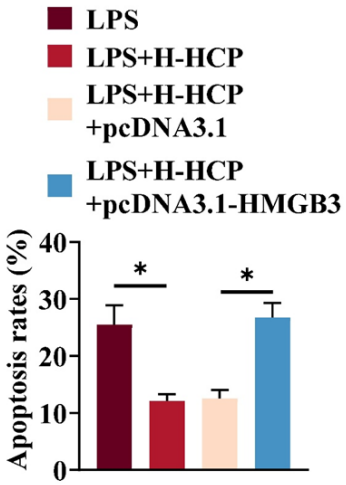

Figure No. 43
Flow cytometry detection of apoptosis in TC-1
Data are expressed as mean ± SD (n=3). *p<0.05

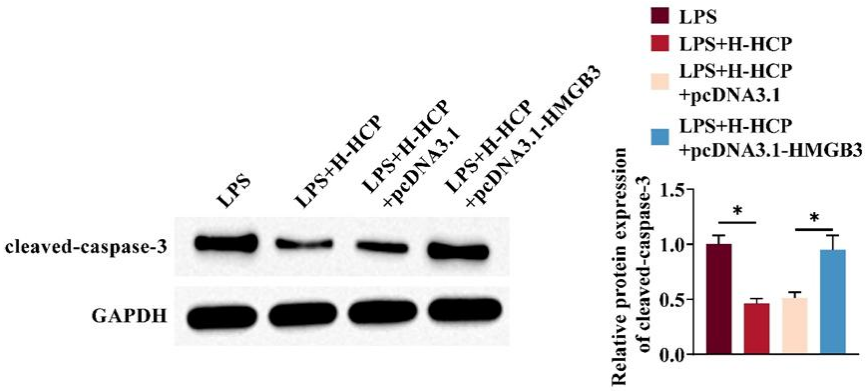

Figure No. 44
Western Blot detection of cleaved caspase-3 expression in TC-1 cells
Data are expressed as mean ± SD (n=3). *p<0.05

DISCUSSION

Pneumonia is widespread in children, and its high incidence and recurrence rate can lead to a variety of serious complications and poor prognosis (Masarweh *et al*., 2021). The current treatment of pneumonia is antiviral, antibacterial and symptomatic supportive therapy (Rogozinski *et al*., 2017). However, the continuous use of antibiotics leads to increased resistance of pathogenic bacteria, making the disease difficult to cure. And excessive inflammatory response can damage the respiratory tract in children. Therefore, it is important to identify the underlying pathogenesis of pneumonia in children and to develop new therapeutic strategies to inhibit its progression.

LPS from Gram-negative bacteria is a potent inflammatory endotoxin that has been associated with many inflammatory lung diseases, stimulates the immune function of the respiratory system, and induces acute and chronic inflammatory responses, leading to pathological changes such as lung injury, emphysema, and airway remodeling, and affecting the development of lungs in children (Bian *et al*., 2022). In the study of Du *et al*. (2012), the volatile extract of *Houttuynia cordata* could repair rapid pulmonary fibrosis by up-regulating IFN-γ and inhibiting TGF-β1/Smad pathway. Therefore, the present study investigated the therapeutic effect of HCP in models of LPS-induced lung injury and evaluated its molecular mechanisms. This research led to the successful creation of an in vivo mouse pneumonia model utilizing LPS. Concurrently, a laboratory-based cell model was developed utilizing TC-1 cells stimulated by LPS. In this study, HCP reduced lung damage caused by LPS in a manner dependent on the dosage, by preventing damage to lung tissues, reducing inflammation, and preventing apoptosis. DEX was also chosen as a positive drug in this study, and its ameliorative effect on pneumonia injury in mice was similar to that of the HCP high-dose group, suggesting that HCP has a favorable ameliorative effect on LPS-induced pneumonia.

Dysregulation of miRNA expression exists in the pathogenesis of pneumonia. miRNAs have been shown to serve as potential diagnostic markers for pneumonia (Huang *et al*., 2019) and are involved in the pathological process of pneumonia (Liu *et al*., 2020). miR-200b-3p, a member of the miR-200 family, is involved in a variety of biological events, such as angiogenesis, cell migration, organ fibrosis and regulation of inflammatory cytokine secretion (Cao *et al*., 2018; Ladak *et al*., 2019). Duan *et al*. found that miR-200b-3p regulated LPS-induced inflammation in human non-small cell lung cancer cell line A549 cells (Duan *et al*., 2021). In this study, miR-200b-3p expression was down-regulated in LPS-induced pneumonia, but administration of HCP treatment was able to up-regulate its expression level in lung tissues and cells. In addition, knockdown of miR-200b-3p inhibited the therapeutic effects of HCP on lung injury in terms of decreasing cell viability and promoting cell inflammation and apoptosis.

miRNAs regulate their downstream target genes by binding to the 3′UTR and are involved in cell proliferation, migration, apoptosis, as well as in intrinsic immunity, inflammation, and infection. HMGB3 is a multifunctional protein and is a key downstream target of a variety of miRNAs. HMGB3 accelerates NSCLC cell viability, colony formation and reduced apoptosis (Song *et al*., 2019). miR-128-3p could target and regulate HMGB3 in acute lung

injury in septic rats (Sun *et al*., 2021). miR-424-5p has a binding site for HMGB3 and is involved in LPS-induced inflammation and apoptosis in human alveolar epithelial cells (Li *et al*., 2023). In this study, HMGB3 was highly expressed in tissues and cells with LPS-induced pneumonia and activated the JNK pathway, but its expression was reduced upon HCP treatment. In addition, miR-200b-3p targeted and inhibited HMGB3, and overexpression of HMGB3 suppressed the protective effects of HCP treatment and miR-200b-3p on LPS-injured lung cells. However, further studies on the role of HCP in clinical practice and detailed physiological mechanisms are still needed.

In summary, HCP was able to reduce inflammatory infiltration and pathological changes in mouse lung tissues, decrease inflammation and apoptosis in lung tissues, and decrease inflammatory factor levels in BALF. HCP treatment also increased lung cell viability, decreased inflammatory factor levels and apoptotic protein expression in TC-1 cells, and ameliorated LPS-induced lung injury. Notably, these therapeutic effects could be realized through the miR-200b-3p/HMGB3/JNK axis.

Competing interests

The authors have no conflicts of interest to declare.

Ethics statement

All animal experiments were complied with the ARRIVE guidelines and performed in accordance with the National Institutes of Health Guide for the Care and Use of Laboratory Animals. The experiments were approved by the Institutional Animal Care and Use Committee of Shandong Provincial Third Hospital (No.SD20210108-1).

REFERENCES

Alaaeldin R, Bakkar SM, Mohyeldin RH, Ali FEM, Abdel-Maqsoud NMR, Fathy M. 2023. Azilsartan modulates HMGB1/NF-kappaB/p38/ERK1/2/JNK and apoptosis pathways during renal ischemia reperfusion injury. **Cells** 12. **https://doi.org/10.3390/cells12010185**

Bian XX, Zhao X, Ma CH, Shen CP. 2022. Arbutin alleviates LPS induced sepsis pneumonia in mice. **Evid Based Complement Alternat Med** 2022: 5863952. **https://doi.org/10.1155/2022/5863952**

Cao Y, Liu Y, Ping F, Yi L, Zeng Z, Li Y. 2018. miR-200b/c attenuates lipopolysaccharide-induced early pulmonary fibrosis by targeting ZEB1/2 via p38 MAPK and TGF-beta/smad3 signaling pathways. **Lab Invest** 98: 339 - 359. **https://doi.org/10.1038/labinvest.2017.123**

Chen MY, Li H, Lu XX, Ling LJ, Weng HB, Sun W, Chen DF, Zhang YY. 2019. *Houttuynia cordata* polysaccharide alleviated intestinal injury and modulated intestinal microbiota in H1N1 virus infected mice. **Chin J Nat Med** 17: 187 - 197. **https://doi.org/10.1016/S1875-5364(19)30021-4**

Cheng BH, Chan JY, Chan BC, Lin HQ, Han XQ, Zhou X, Wan DCC, Wang YF, Leung PC, Fung KP, Lau CBS. 2014. Structural characterization and immunomodulatory effect of a polysaccharide HCP-2 from *Houttuynia cordata*. **Carbohydr Polym** 103: 244 - 249. **https://doi.org/10.1016/j.carbpol.2013.12.048**

Cheng D, Sun L, Zou S, Chen J, Mao H, Zhang Y, Liao N, Zhang R. 2019. Antiviral effects of *Houttuynia cordata* polysaccharide extract on murine norovirus-1 (MNV-1)-A human norovirus surrogate. **Molecules** 24. **https://doi.org/10.3390/molecules24091835**

Chun JM, Nho KJ, Kim HS, Lee AY, Moon BC, Kim HK. 2014. An ethyl acetate fraction derived from *Houttuynia cordata* extract inhibits the production of inflammatory markers by suppressing NF-small ka, CyrillicB and MAPK activation in lipopolysaccharide-stimulated RAW 264.7 macrophages. **BMC Complement Altern Med** 14: 234. **https://doi.org/10.1186/1472-6882-14-234**

Du S, Li H, Cui Y, Yang L, Wu J, Huang H, Chen Y, Huang W, Zhang R, Yang J, Chen D, Li Y, Zhang S, Zhou J, Wei Z, Chow NT. 2012. *Houttuynia cordata* inhibits lipopolysaccharide-induced rapid pulmonary fibrosis by up-regulating IFN-gamma and inhibiting the TGF-beta1/Smad pathway. **Int Immunopharmacol** 13: 331 - 340. **https://doi.org/10.1016/j.intimp.2012.03.011**

Duan XY, Sun Y, Zhao ZF, Shi YQ, Ma XY, Tao L, Liu MW. 2021. Baicalin attenuates LPS-induced alveolar type II epithelial cell A549 injury by attenuation of the FSTL1 signaling pathway via increasing miR-200b-3p expression. **Innate Immunol** 27: 294 - 312.

Huang S, Feng C, Zhai YZ, Zhou X, Li B, Wang LL, Chen W, Lv FQ, Li TS. 2017. Identification of miRNA biomarkers of pneumonia using RNA-sequencing and bioinformatics analysis. **Exp Ther Med** 13: 1235 - 1244. **https://doi.org/10.3892/etm.2017.4151**

Huang F, Bai J, Zhang J, Yang D, Fan H, Huang L, Shi T, Lu G. 2019. Identification of potential diagnostic biomarkers for pneumonia caused by adenovirus infection in children by screening serum exosomal microRNAs. **Mol Med Rep** 19: 4306 - 4314. **https://doi.org/10.3892/mmr.2019.10107**

Ju IG, Lee S, Choi JG, Kim N, Huh E, Lee JK, Oh MS. 2023. Affiliations aerial part of *Houttuynia cordata* reverses memory impairment by regulating amyloid beta accumulation and neuroinflammation in Alzheimer's disease model. **Phytother Res** 37: 2854 - 2863. **https://doi.org/10.1002/ptr.7781**

Ladak SS, Roebuck E, Powell J, Fisher AJ, Ward C, Ali S. 2019. The role of miR-200b-3p in modulating TGF-beta1-induced injury in human bronchial epithelial cells. **Transplantation** 103: 2275 - 2286. **https://doi.org/10.1097/TP.0000000000002845**

Lee JH, Ahn J, Kim JW, Lee SG, Kim HP. 2015. Flavonoids from the aerial parts of *Houttuynia cordata* attenuate lung inflammation in mice. **Arch Pharm Res** 38: 1304 - 1311. **https://doi.org/10.1007/s12272-015-0585-8**

Li J, Liu S. 2020. LncRNA GAS5 suppresses inflammatory responses and apoptosis of alveolar epithelial cells by targeting miR-429/DUSP1. **Exp Mol Pathol** 113: 104357. **https://doi.org/10.1016/j.yexmp.2019.104357**

Li Y, Zhang C, Zhao Z. 2023. CircSLCO3A1 depletion ameliorates lipopolysaccharide-induced inflammation and apoptosis of human pulmonary alveolar epithelial cells through the miR-424-5p/HMGB3 pathway. **Mol Cell Toxicol** 2023: 1 - 12. **https://doi.org/10.1007/s13273-023-00341-6**

Liu M, Li W, Song F, Zhang L, Sun X. 2020. Silencing of lncRNA MIAT alleviates LPS-induced pneumonia via regulating miR-147a/NKAP/NF-kappaB axis. **Aging** 13: 2506 - 2518. **https://doi.org/10.18632/aging.202284**

Lu Y, Jiang Y, Ling L, Zhang Y, Li H, Chen D. 2018. Beneficial effects of *Houttuynia cordata* polysaccharides on "two-hit" acute lung injury and endotoxic fever in rats associated with anti-complementary activities. **Acta Pharm Sin B** 8: 218 - 227. **https://doi.org/10.1016/j.apsb.2017.11.003**

Masarweh K, Gur M, Toukan Y, Bar-Yoseph R, Kassis I, Gut G, Hakim F, Nir V, Bentur L. 2021. Factors associated with complicated pneumonia in children. **Pediatr Pulmonol** 56: 2700 - 2706. **https://doi.org/10.1002/ppul.25468**

Postma DF, van Werkhoven CH, van Elden LJ, Thijsen SF, Hoepelman AI, Kluytmans JA, Boersma WG, Compaijen CJ, van der Wall E, Prins JM, Oosterheert JJ, Bonten MJM, CAP-START Study Group. 2015. Antibiotic treatment strategies for community-acquired pneumonia in adults. **N Engl J Med** 372: 1312 - 1323. **https://doi.org/10.1056/NEJMoa1406330**

Rogozinski LE, Alverson BK, Biondi EA. 2017. Diagnosis and treatment of *Mycoplasma pneumoniae* in children. **Minerva Pediatr** 69: 156 - 160. **https://doi.org/10.23736/S0026-4946.16.04866-0**

Song N, Wang B, Feng G, Duan L, Yuan S, Jia W, Liu Y. 2019. Knockdown of high mobility group box 3 impairs cell viability and colony formation but increases apoptosis in A549 human non-small cell lung cancer cells. **Oncol Lett** 17: 2937 - 2945. **https://doi.org/10.3892/ol.2019.9927**

Sun J, Xin K, Leng C, Ge J. 2021. Down-regulation of SNHG16 alleviates the acute lung injury in sepsis rats through miR-128-3p/HMGB3 axis. **BMC Pulm Med** 21: 191. **https://doi.org/10.1186/s12890-021-01552-0**

Taniguchi N, Kawakami Y, Maruyama I, Lotz M. 2018. HMGB proteins and arthritis. **Hum Cell** 31: 1 - 9. **https://doi.org/10.1007/s13577-017-0182-x**

Ullah S, John P, Bhatti A. 2014. MicroRNAs with a role in gene regulation and in human diseases. **Mol Biol Rep** 41: 225 - 232. **https://doi.org/10.1007/s11033-013-2855-1**

Wang Z, Liao Y, Wang L, Lin Y, Ye Z, Zeng X, Liu X, Wei F, Yang N. 2020. Small RNA deep sequencing reveals novel miRNAs in peripheral blood mononuclear cells from patients with IgA nephropathy. **Mol Med Rep** 22: 3378 - 3386. **https://doi.org/10.3892/mmr.2020.11405**

Wang S, Chen X, Cheng J, Cai T, Wu X, Cheng Z, Qi S, Qi Z. 2021a. Calunduloside E inhibits HepG2 cell proliferation and migration via p38/JNK-HMGB1 signalling axis. **J Pharmacol Sci** 147: 18 - 26. **https://doi.org/10.1016/j.jphs.2021.05.005**

Wang X, Guo P, Tian J, Li J, Yan N, Zhao X, Ma Y. 2021b. LncRNA GAS5 participates in childhood pneumonia by inhibiting cell apoptosis and promoting SHIP-1 expression via downregulating miR-155. **BMC Pulm Med** 21: 362. **https://doi.org/10.1186/s12890-021-01724-y**

Xu YY, Zhang YY, Ou YY, Lu XX, Pan LY, Li H, Lu Y, Chen DF. 2015. Houttuyniacordata Thunb. polysaccharides ameliorates lipopolysaccharide-induced acute lung injury in mice. **J Ethnopharmacol** 173: 81 - 90.

https://doi.org/10.1016/j.jep.2015.07.015

Yang H, Dong Y, Zhou Y, Li H. 2021. Overexpression of miR-874-3p alleviates LPS-induced apoptosis and inflammation in alveolar epithelial cell by targeting EGR3/NF-kappaB. **Acta Biochim Pol** 68: 231 - 238. **https://doi.org/10.18388/abp.2020_5523**

Yu Z, Tong Y, Zhang R, Ding X, Li Q. 2017. Saquinavir ameliorates liver warm ischemia-reperfusion-induced lung injury via HMGB-1- and P38/JNK-mediated TLR-4-dependent signaling pathways. **Mediators Inflamm** 2017: 7083528. **https://doi.org/10.1155/2017/7083528**

Zhou L, Jiao Y, Tang J, Zhao Z, Zhu H, Lu Y, Chen D. 2022. Ultrafiltration isolation, structure and effects on H1N1-induced acute lung injury of a heteropolysaccharide from *Houttuynia cordata*. **Int J Biol Macromol** 222: 2414 - 2425. **https://doi.org/10.1016/j.ijbiomac.2022.10.027**

Zhu H, Lu X, Ling L, Li H, Ou Y, Shi X, Lu Y, Zhang Y, Chen D. 2018. *Houttuynia cordata* polysaccharides ameliorate pneumonia severity and intestinal injury in mice with influenza virus infection. **J Ethnopharmacol** 218: 90 - 99. **https://doi.org/10.1016/j.jep.2018.02.016**